An *sp*-hybridized molecular carbon allotrope, cyclo[18]carbon

Katharina Kaiser,[1†] Lorel M. Scriven,[2†] Fabian Schulz,[1] Przemyslaw Gawel,[2*] Leo Gross,[1*] Harry L. Anderson[2*]

[1] IBM Research–Zurich, Säumerstrasse 4, 8803 Rüschlikon, Switzerland

[2] Department of Chemistry, Oxford University, Chemistry Research Laboratory, Oxford, OX1 3TA, United Kingdom

[†] These authors contributed equally.

*Corresponding authors. Email: przemyslaw.gawel@chem.ox.ac.uk; lgr@zurich.ibm.com; harry.anderson@chem.ox.ac.uk

Abstract:

Carbon allotropes built from rings of two-coordinate atoms, known as cyclo[*n*]carbons, have fascinated chemists for many years, but until now they could not be isolated or structurally characterized, due to their high reactivity. We generated cyclo[18]carbon (C_{18}) using atom manipulation on bilayer NaCl on Cu(111) at 5 Kelvin by eliminating carbon monoxide from a cyclocarbon oxide molecule $C_{24}O_6$. Characterization of cyclo[18]carbon by high-resolution atomic force microscopy revealed a polyynic structure with defined positions of alternating triple and single bonds. The high reactivity of cyclocarbon and cyclocarbon oxides allows covalent coupling between molecules to be induced by atom manipulation, opening an avenue for the synthesis of other carbon allotropes and carbon-rich materials from the coalescence of cyclocarbon molecules.

One Sentence Summary: Cyclo[18]carbon has been synthesized on bilayer NaCl on Cu(111) at 5 K, and characterized by atomic force microscopy, revealing its polyynic structure.

The discovery of fullerenes (1), carbon nanotubes (2), and graphene (3), all of which consist exclusively of 3-coordinate carbon atoms, has sparked a new field of synthetic carbon allotropes (4, 5). The only molecular allotropes of carbon that have been isolated are the fullerenes (1). Rings of 2-coordinate carbon atoms (cyclo[*n*]carbons, C_n) have been suggested as an alternative family of molecular carbon allotropes (4-6). There is evidence for the existence of cyclocarbons in the gas phase (4, 5, 7, 8), but these highly reactive species have not been structurally characterized or studied in condensed phases. Whether cyclocarbons are polyynic, with alternating single and triple bonds of different lengths (D_{9h} symmetry), or cumulenic with consecutive double bonds (D_{18h} symmetry, see Fig. 1) is fundamental and controversial (9-12).

A distinctive feature of *sp*-hybridized carbon allotropes is that they possess two perpendicular π-conjugated electron systems (Fig. 1). Hückel's rule predicts for planar, cyclic conjugated systems with $(4n + 2)$ π electrons an aromatic structure with no bond length alternation (BLA) (13). Hoffmann predicted, in 1966, that two orthogonal ring currents would be formed in C_{18}, causing double aromatic stabilization (6). Since then, the structures of cyclo[*n*]carbons have been a topic of theoretical debate, and the results depend on the level of theory (9, 10, 13). Most density functional theory (DFT) and Møller-Plesset perturbation theory calculations predict that the lowest energy geometry of C_{18} is cumulenic D_{18h} (9, 10), whereas Hartree-Fock (4) and high-level Monte Carlo and coupled cluster methods predict that the polyyne D_{9h} form is the ground state (11, 12).

Most attempts at synthesizing cyclocarbons have used a masked alkyne equivalent incorporated into a cyclic precursor designed to generate cyclo[*n*]carbon when activated by heat or light. Methods of unmasking included a retro-Diels-Alder reaction (4), decomplexation (14), decarbonylation (15) and [2+2] cycloreversion (16). These attempts have given tantalizing glimpses of cyclo[*n*]carbon in the gas phase. Cyclo[*n*]carbons may coalescence to form fullerenes (8, 15), and gas-phase electronic spectra of C_{18}, formed by laser ablation of graphite, have been measured, but these studies did not reveal whether the structures are cumulenic or polyynic (17).

An alternative approach for studying highly reactive molecules is to isolate them on an inert surface at low temperature. Developments in the field of scanning tunneling microscopy (STM) and atomic force microscopy (AFM), in particular tip functionalization, have enabled

imaging of molecules with unprecedented resolution (18, 19), and atom manipulation can trigger chemical reactions on surfaces (19-22). We report the synthesis and structural characterization of cyclo[18]carbon. A low-temperature STM-AFM was used to sequentially remove masking CO groups from the precursor $C_{24}O_6$ by atom manipulation (Fig. 2). We resolved the structure of cyclo[18]carbon and observed BLA in its ground state. We also demonstrated covalent fusion by atom manipulation of cyclocarbon oxides, exploiting their high reactivity.

Cyclocarbon oxides, developed by Diederich and co-workers, were selected as suitable candidates for on-surface cyclocarbon generation (14). We synthesized the cyclocarbon oxide $C_{24}O_6$ using procedures similar to those previously reported (for synthetic details and NMR spectra see supplementary material and figs. S1-S7) and sublimed it from a Si wafer onto a cold ($T \approx 10$ K) Cu(111) surface partially covered with (100)-oriented bilayer NaCl islands. All molecules were studied on bilayer NaCl, providing an inert surface on which radicals and polyynes (22) are stable and can be imaged (19). The experiments were carried out in a combined STM/AFM system equipped with a qPlus force sensor (23) operating at $T = 5$ K in frequency-modulation mode (24). We used CO tip functionalization to improve the resolution (18). AFM images were acquired at constant height, with the offset Δz applied to the tip-sample distance with respect to the STM setpoint above the bare NaCl surface. We simulated AFM images using the probe particle model (25) based on the structures relaxed in the gas phase, calculated by DFT (see also supplementary text).

After deposition, we found molecules of the precursor $C_{24}O_6$ on the NaCl surface, as well as some fragmented or (partially) decarbonylated molecules and single CO molecules (see supplementary material fig. S8 for an overview image). This result indicated that partial decarbonylation and dissociation took place during sublimation. Figure 3 shows AFM data and corresponding simulations for $C_{24}O_6$ and products created by atom manipulation (STM images are shown in fig. S9). $C_{24}O_6$ molecules appeared as triangular objects with dark features at the corners and two bright protrusions at each side (Fig. 3B). The dark contrast, characteristic of ketone groups (26) was explained by a reduced adsorption height and a relatively small electron density in the region imaged above the O atoms, which have high electron affinity. Both effects led to comparably small Pauli repulsive forces above the O atoms (26). Figure 3B was recorded at moderate tip height ("AFM far"), at which differences in bond order were visible in the Δf signal, with high brightness, i.e., high Δf indicating high bond order (27). The two bright features

at each side of the molecule were assigned to triple bonds (22, 28). At decreased tip-sample distance ("AFM close", Fig. 3C), repulsive forces made greater contributions and tip relaxations, i.e., tilting of the CO at the tip apex, affected the AFM images substantially. These effects led to apparent sharpening of the bonds, and pronounced differences in apparent bond lengths (25, 27, 29). The different contrasts of the three different sides of $C_{24}O_6$ (Fig. 3B) suggest an adsorption geometry not parallel to the surface (26).

To decarbonylate $C_{24}O_6$, the tip was positioned in the vicinity (a few nanometers) of the molecule, retracted by about 3 Å from the STM setpoint (typically $V = 0.2$ V and $I = 0.5$ pA) and the sample bias voltage V was increased to about $V = +3$ V, for a few seconds. This procedure often led to the removal of two, four, or six CO moieties. Because of the nonlocality and the observed bias thresholds (see supplementary text), we tentatively propose that the reaction was mediated by inelastic electron tunneling through hot interface state electrons (19). The most abundant products were $C_{22}O_4$ (Fig. 3F) and $C_{20}O_2$ (Fig. 3K). The removal of a masking group (2 CO) resulted in the formation of a longer bent polyynic segment.

Assigning the bright features in the "AFM far" images to the location of triple bonds, we observed curved polyyne segments with the expected number of triple bonds: 5 in $C_{22}O_4$ (Fig. 3G) and 8 in $C_{20}O_2$ (Fig. 3L). At small tip height (Fig. 3, H and M), we observed sharp bond-like features with corners at the assigned positions of triple bonds and straight lines in between. This contrast was explained by CO tip relaxation, in that maxima in the potential energy landscape, from which the tip apex was repelled, were located above the triple bonds because of their high electron density. In between these maxima, ridges in the potential landscape led to straight bond-like features (25, 30, 31). The assignment of the intermediates was further supported by AFM simulations (Fig. 3, 4^{th} and 5^{th} column) and STM images within the fundamental gap and at the ion resonances (see supplementary material figs. S10-S13).

We removed all six CO moieties from $C_{24}O_6$, with 13% yield (calculated by evaluation of 90 atomic manipulation events; for details on the statistics and procedure for on-surface decarbonylation, see supplementary text, table S1), typically resulting in circular molecules (Fig. 3, Q and R). At moderate tip heights (Fig. 3Q) the resulting molecule exhibited a cyclic arrangement of nine bright lobes. One side of the molecule appeared brighter, indicating that its adsorption geometry was not parallel to the surface (see supplementary fig. S14). For smaller tip

heights (Fig. 3R), the molecule appeared as a nonagon with corners at the positions of the bright lobes that were observed at larger tip-sample distance (Fig. 3Q). The contrast can be explained in analogy to the precursors: The bright lobes in Fig. 3Q and the corresponding corners in Fig. 3R were observed above triple bonds. The molecule was thus identified as cyclo[18]carbon. The AFM contrast provided evidence for a polyynic structure of cyclo[18]carbon on NaCl with the defined positions of triple bonds supported by AFM simulations (Fig. 3, S and T and fig. S15). In the case of a D_{18h} cumulenic structure, no BLA and an 18-fold symmetry of the molecule would be expected, in contrast to the experimental result.

In the ninefold symmetric form described above, the cyclo[18]carbon molecule was uncharged (neutral). We found that cyclo[18]carbon exhibited charge bistability (32) on this surface and it changed to a less symmetric and less planar geometry in the negatively charged state. The molecule could be reversibly switched between its two charge states and associated geometries (figs. S16-S18). During charge-state switching, tip-induced decarbonylation, and STM imaging, the molecules often jumped to different locations on the surface, indicating a very small diffusion barrier on NaCl. Cyclo[18]carbon moved more frequently than the other molecules observed, and it was often found adjacent to step edges or individual CO molecules adsorbed on the surface, pinning the molecule (Fig. 3, Q and R).

The high reactivity of cyclo[18]carbon and its oxides makes them promising candidates for on-surface covalent molecular fusion by atom manipulation, of which very few previous examples have been reported (20). Applying an elevated bias voltage near two proximate molecules led to their fusion. For example, the two neighboring cyclocarbon oxide intermediates, $C_{20}O_2$ and $C_{22}O_4$ (Fig. 4A), were fused in this way. After constant-current imaging at a set point of $V = 3$ V and $I = 0.5$ pA, the molecules reacted through a [4+2] cycloaddition, as revealed by the AFM resolved structure of the product shown in Fig. 4C (see fig. S19 for a possible mechanism and figs. S20-S21 for more examples of on-surface fused molecules). These results demonstrated that the strained polyynic moieties of cyclo[18]carbon and its oxide intermediates allowed covalent coupling by atom manipulation. Our results provide direct experimental insights into the structure of a cyclocarbon and open the way to create other elusive carbon-rich molecules by atom manipulation.

References

[1] H. W. Kroto, J. R. Heath, S. C. O'Brien, R. F. Curl, R. E. Smalley, C_{60}: Buckminsterfullerene, *Nature* **318**, 162–163 (1985).

[2] S. Iijima, T. Ichihashi, Single-shell carbon nanotubes of 1-nm diameter, *Nature* **363**, 603–605 (1993).

[3] K. S. Novoselov, A. K. Geim, S. V. Morozov, D. Jiang, Y. Zhang, S. V. Dubonos, I. V. Grigorieva, A. A. Firsov, Electric field effect in atomically thin carbon films, *Science* **306**, 666–669 (2004).

[4] F. Diederich, Y. Rubin, C. B. Knobler, R. L. Whetten, K. E. Schriver, K. N. Houk, Y. Li, All-carbon molecules: Evidence for the generation of cyclo[18]carbon from a stable organic precursor, *Science* **245**, 1088–1090 (1989).

[5] F. Diederich, M. Kivala, All-carbon scaffolds by rational design, *Adv. Mater.* **22**, 803–812 (2010).

[6] R. Hoffmann, Extended Hückel theory—v: Cumulenes, polyenes, polyacetylenes and C_n, *Tetrahedron* **22**, 521–538 (1966).

[7] S. W. McElvany, M. M. Ross, N. S. Goroff, F. Diederich, Cyclocarbon coalescence: Mechanisms for tailor-made fullerene formation, *Science* **259**, 1594–1596 (1993).

[8] G. von Helden, N. G. Gotts, M. T. Bowers, Experimental evidence for the formation of fullerenes by collisional heating of carbon rings in the gas phase, *Nature* **363**, 60–63 (1993).

[9] V. Parasuk, J. Almlof, M. W. Feyereisen, The [18] all-carbon molecule: Cumulene or polyacetylene?, *J. Am. Chem. Soc.* **113**, 1049–1050 (1991).

[10] C. Neiss, E. Trushin, A. Görling, The nature of one-dimensional carbon: Polyynic versus cumulenic, *ChemPhysChem* **15**, 2497–2502 (2014).

[11] T. Torelli, L. Mitas, Electron correlation in C_{4N+2} carbon rings: Aromatic versus dimerized structures, *Phys. Rev. Lett.* **85**, 1702–1705 (2000).

[12] S. Arulmozhiraja, T. Ohno, CCSD calculations on C_{14}, C_{18}, and C_{22} carbon clusters, *J. Chem. Phys.* **128**, 114301 (2008).

[13] P. W. Fowler, N. Mizoguchi, D. E. Bean, R. W. A. Havenith, Double aromaticity and ring currents in all-carbon rings, *Chem. Eur. J.* **15**, 6964–6972 (2009).

[14] Y. Rubin, C. B. Knobler, F. Diederich, Synthesis and crystal structure of a stable hexacobalt complex of cyclo[18]carbon, *J. Am. Chem. Soc.* **112**, 4966–4968 (1990).

[15] Y. Rubin, M. Kahr, C. B. Knobler, F. Diederich, C. L. Wilkins, The higher oxides of carbon $C_{8n}O_{2n}$ (n = 3–5): synthesis, characterization, and X-ray crystal structure. Formation of cyclo[n]carbon ions C_n^+ (n = 18, 24), C_n^- (n = 18, 24, 30), and higher carbon ions including C_{60}^+ in laser desorption Fourier transform mass spectrometric experiments, *J. Am. Chem. Soc.* **113**, 495–500 (1991).

[16] Y. Tobe, H. Matsumoto, K. Naemura, Y. Achiba, T. Wakabayashi, Generation of cyclocarbons with 4*n* carbon atoms (C_{12}, C_{16}, and C_{20}) by [2 + 2] cycloreversion of propellane-annelated dehydroannulenes, *Angew. Chem. Int. Ed.* **35**, 1800–1802 (1996).

[17] A. E. Boguslavskiy, H. Ding, J. P. Maier, Gas-phase electronic spectra of C_{18} and C_{22} rings, *J. Chem. Phys.* **123**, 034305 (2005).

[18] L. Gross, F. Mohn, N. Moll, P. Liljeroth, G. Meyer, The Chemical Structure of a Molecule Resolved by Atomic Force Microscopy, *Science* **325**, 1110–1114 (2009).

[19] N. Pavliček, L. Gross, Generation, manipulation and characterization of molecules by atomic force microscopy, *Nat. Rev. Chem.* **1**, 0005 (2017).

[20] S.-W. Hla, L. Bartels, G. Meyer, K.-H. Rieder, Inducing all steps of a chemical reaction with the scanning tunneling microscope tip: Towards single molecule engineering, *Phys. Rev. Lett.* **85**, 2777–2780 (2000).

[21] J. Repp, G. Meyer, S. Paavilainen, F. E. Olsson, M. Persson, Imaging Bond Formation Between a Gold Atom and Pentacene on an Insulating Surface, *Science* **312**, 1196–1199 (2006).

[22] N. Pavliček, P. Gawel, D. R. Kohn, Z. Majzik, Y. Xiong, G. Meyer, H. L. Anderson, L. Gross, Polyyne formation via skeletal rearrangement induced by atomic manipulation, *Nat. Chem.* **10**, 853–858 (2018).

[23] F. J. Giessibl, High-speed force sensor for force microscopy and profilometry utilizing a quartz tuning fork, *Appl. Phys. Lett.* **73**, 3956–3958 (1998).

[24] T. R. Albrecht, P. Grütter, D. Horne, D. Rugar, Frequency modulation detection using high-Q cantilevers for enhanced force microscope sensitivity, *J. Appl. Phys.* **69**, 668–673 (1991).

[25] P. Hapala, G. Kichin, C. Wagner, F. S. Tautz, R. Temirov, P. Jelínek, Mechanism of high-resolution STM/AFM imaging with functionalized tips, *Phys. Rev. B* **90**, 085421 (2014).

[26] B. Schuler, W. Liu, A. Tkatchenko, N. Moll, G. Meyer, A. Mistry, D. Fox, L. Gross, Adsorption geometry determination of single molecules by atomic force microscopy, *Phys. Rev. Lett.* **111**, 106103 (2013).

[27] L. Gross, F. Mohn, N. Moll, B. Schuler, A. Criado, E. Guitián, D. Peña, A. Gourdon, G. Meyer, Bond-order discrimination by atomic force microscopy, *Science* **337**, 1326–1329 (2012).

[28] D. G. de Oteyza, P. Gorman, Y.-C. Chen, S. Wickenburg, A. Riss, D. J. Mowbray, G. Etkin, Z. Pedramrazi, H.-Z. Tsai, A. Rubio, M. F. Crommie, F. R. Fischer, Direct imaging of covalent bond structure in single-molecule chemical reactions, *Science* **340**, 1434–1437 (2013).

[29] A. Riss, S. Wickenburg, P. Gorman, L. Z. Tan, H.-Z. Tsai, D. G. de Oteyza, Y.-C. Chen, A. J. Bradley, M. M. Ugeda, G. Etkin, S. G. Louie, F. R. Fischer, M. F. Crommie, Local electronic and chemical structure of oligo-acetylene derivatives formed through radical cyclizations at a surface, *Nano Lett.* **14**, 2251–2255 (2014).

[30] N. Pavliček, B. Fleury, M. Neu, J. Niedenführ, C. Herranz-Lancho, M. Ruben, J. Repp, Atomic force microscopy reveals bistable configurations of dibenzo[a,h]thianthrene and their interconversion pathway, *Phys. Rev. Lett.* **108**, 086101 (2012).

[31] S. K. Hämäläinen, N. van der Heijden, J. van der Lit, S. den Hartog, P. Liljeroth, I. Swart, Intermolecular contrast in atomic force microscopy images without intermolecular bonds, *Phys. Rev. Lett.* **113**, 186102 (2014).

[32] I. Swart, T. Sonnleitner, J. Repp, Charge state control of molecules reveals modification of the tunneling barrier with intramolecular contrast, *Nano Lett.* **11**, 1580–1584 (2011).

[33] R. Bennewitz, V. Barwich, M. Bammerlin, C. Loppacher, M. Guggisberg, A. Baratoff, E. Meyer, H.-J. Güntherodt, Ultrathin films of NaCl on Cu(111): A LEED and dynamic force microscopy study, *Surf. Sci.* **438**, 289–296 (1999).

[34] L. Bartels, G. Meyer, K.-H. Rieder, Controlled vertical manipulation of single CO molecules with the scanning tunneling microscope: A route to chemical contrast, *Appl. Phys. Lett.* **71**, 213–215 (1997).

[35] B. Schuler, G. Meyer, D. Peña, O. C. Mullins, L. Gross, Unraveling the molecular structures of asphaltenes by atomic force microscopy, *J. Am. Chem. Soc.* **137**, 9870–9876 (2015).

[36] Y. Rubin, T. C. Parker, S. J. Pastor, S. Jalisatgi, C. Boulle, C. L. Wilkins, Acetylenic cyclophanes as fullerene precursors: formation of $C_{60}H_6$ and C_{60} by laser desorption mass spectrometry of $C_{60}H_6(CO)_{12}$, *Angew. Chem. Int. Ed.* **37**, 1226–1229 (1998).

[37] R. Keller, H. Wycoff, L. E. Marchi, Copper(I) Chloride, *Inorg. Synth.* **2**, 1–4 (1946).

[38] A. J. Weymouth, T. Hofmann, F. J. Giessibl, Quantifying molecular stiffness and interaction with lateral force microscopy, *Science* **343**, 1120–1122 (2014).

[39] M. Ellner, N. Pavliček, P. Pou, B. Schuler, N. Moll, G. Meyer, L. Gross, R. Peréz, The electric field of CO tips and its relevance for atomic force microscopy, *Nano Lett.* **16**, 1974–1980 (2016).

[40] T. Leoni, O. Guillermet, H. Walch, V. Langlais, A. Scheuermann, J. Bonvoisin, S. Gauthier, Controlling the charge state of a single redox molecular switch, *Phys. Rev. Lett.* **106**, 216103 (2011).

[41] J. Repp, G. Meyer, F. E. Olsson, M. Persson, Controlling the charge state of individual gold adatoms, *Science* **305**, 493–495 (2004).

[42] J. Repp, G. Meyer, S. Paavilainen, F. E. Olsson, M. Persson, Scanning Tunneling Spectroscopy of Cl Vacancies in NaCl Films: Strong Electron-Phonon Coupling in Double-Barrier Tunneling Junctions, *Phys. Rev. Lett.* **95**, 225503 (2005).

[43] J. Repp, G. Meyer, K.-H. Rieder, Snell's law for surface electrons: Refraction of an electron gas imaged in real space, *Phys. Rev. Lett.* **92**, 036803 (2004).

[44] V. Schendel, B. Borca, I. Pentegov, T. Michnowicz, U. Kraft, H. Klauk, P. Wahl, U. Schlickum, K. Kern, Remotely controlled isomer selective molecular switching, *Nano Lett.* **16**, 93–97 (2016).

[45] J. N. Ladenthin, L. Grill, S. Gawinkowski, S. Liu, J. Waluk, T. Kumagai, Hot carrier-induced tautomerization within a single porphycene molecule on Cu (111), *ACS Nano* **9**, 7287–7295 (2015).

[46] N. Pavliček, Z. Majzik, S. Collazos, G. Meyer, D. Pérez, E. Guitian, D. Peña, L. Gross, Generation and characterization of a *meta*-aryne on Cu and NaCl surfaces, *ACS Nano* **11**, 10768–10773 (2017).

[47] V. Blum, R. Gehrke, F. Hanke, P. Havu, V. Havu, X. Ren, K. Reuter, M. Scheffler, *Ab initio* molecular simulations with numeric atom-centered orbitals, *Comput. Phys. Commun.* **180**, 2175–2196 (2009).

[48] J. P. Perdew, K. Burke, M. Ernzerhof, Generalized gradient approximation made simple, *Phys. Rev. Lett.* **77**, 3865–3868 (1996).

[49] J. Heyd, G. E. Scuseria, M. Ernzerhof, Hybrid functionals based on a screened coulomb potential, *J. Chem. Phys.* **118**, 8207–8215 (2003).

[50] A. Tkatchenko, M. Scheffler, Accurate molecular van der Waals interactions from groundstate electron density and free-atom reference data, *Phys. Rev. Lett.* **102**, 073005 (2009).

[51] J. van der Lit, F. Di Cicco, P. Hapala, P. Jelinek, I. Swart, Submolecular resolution imaging of molecules by atomic force microscopy: The influence of the electrostatic force, *Phys. Rev. Lett.* **116**, 096102 (2016).

Acknowledgments: We thank Nikolaj Moll and Rolf Allenspach for discussions. **Funding:** We thank the ERC (grant 320969 and 682144) and the Leverhulme Trust (Project Grant RPG-2017-032) for support. P.G. acknowledges the receipt of a Postdoc.Mobility fellowship from the Swiss National Science Foundation (P300P2-177829). **Author contributions:** L.M.S., P.G. and H.L.A. synthesized the precursors; K.K., F.S., L.M.S. and L.G. performed the AFM experiments; F.S., P.G. and K.K. carried out the DFT calculations; F.S. performed the AFM simulations; all authors contributed to conceiving the research and writing the manuscript. **Competing interests:** The authors declare no competing interests. **Data and materials availability:** All data needed to evaluate the conclusions in the paper are available in the main text or the supplementary materials.

Figure Captions:

Figure 1. Two possible structures of cyclo[18]carbon: the polyynic form with D_{9h} symmetry and the cumulenic form with D_{18h} symmetry, (BLA = bond length alternation) and visualization of their perpendicular π-systems.

Figure 2: Reaction scheme for the on-surface formation of C_{18}. Decarbonylation was achieved *via* voltage pulses resulting in the loss of two, four or six CO moieties.

Figure 3: Precursor and products generated by tip-induced decarbonylation. Structures (1st column) and AFM images (2nd and 3rd column) recorded with a CO-functionalized tip at different tip offsets Δz, with respect to an STM set point of $I = 0.5$ pA, $V = 0.2$ V above the NaCl surface, showing (**A**–**E**) precursor, (**F**–**J** and **K**–**O**) most frequently observed intermediates and (**P**–**T**) cyclo[18]carbon. The bright features at the lower part in L, M, Q and R correspond to individual CO molecules. Simulated AFM images (4th and 5th column) based on gas-phase DFT calculated geometries. The difference in probe height in "sim. far" to "sim. close" corresponds to the respective differences in "AFM far" and "AFM close". The same scale bar as in (B) applies to all experimental and simulated AFM images.

Figure 4: Molecular fusion by atom manipulation. (**A**) STM image of two neighboring intermediates, identified as $C_{22}O_4$ and $C_{20}O_2$. Imaging the area at constant current (c.c.) with a set point of $V = 3$ V, $I = 0.5$ pA resulted in the reaction between the molecules. (**B**, **C**) STM and AFM image of the resulting fused molecule, respectively. (**D**) Proposed reaction scheme. See supplementary material for further examples of molecular fusion reactions.

Supplementary Materials:

Materials and Methods

Supplementary Text SM1

Table S1

Figs. S1 to S21

Reference 33 to 51

Graphics, Figures 1–4 for main text

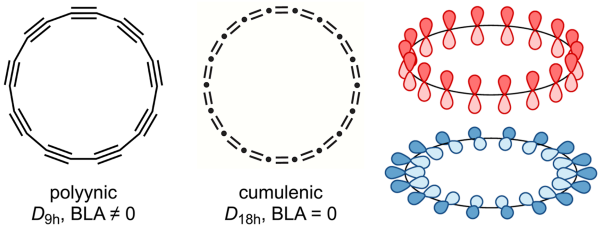

Figure 1. Two possible structures of cyclo[18]carbon: the polyynic form with D_{9h} symmetry and the cumulenic form with D_{18h} symmetry, (BLA = bond length alternation) and visualization of their perpendicular π-systems.

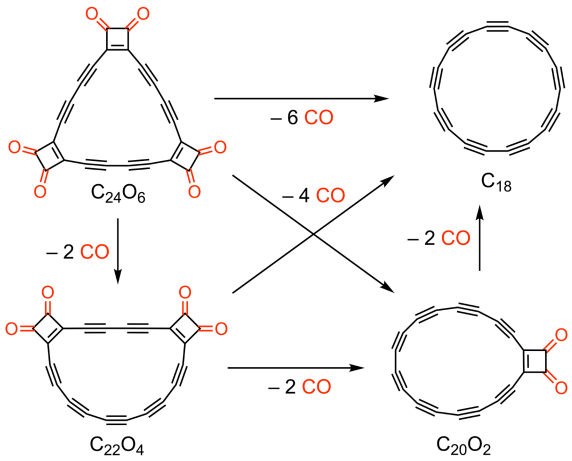

Figure 2: Reaction scheme for the on-surface formation of C_{18}. Decarbonylation was achieved *via* voltage pulses resulting in the loss of two, four or six CO moieties.

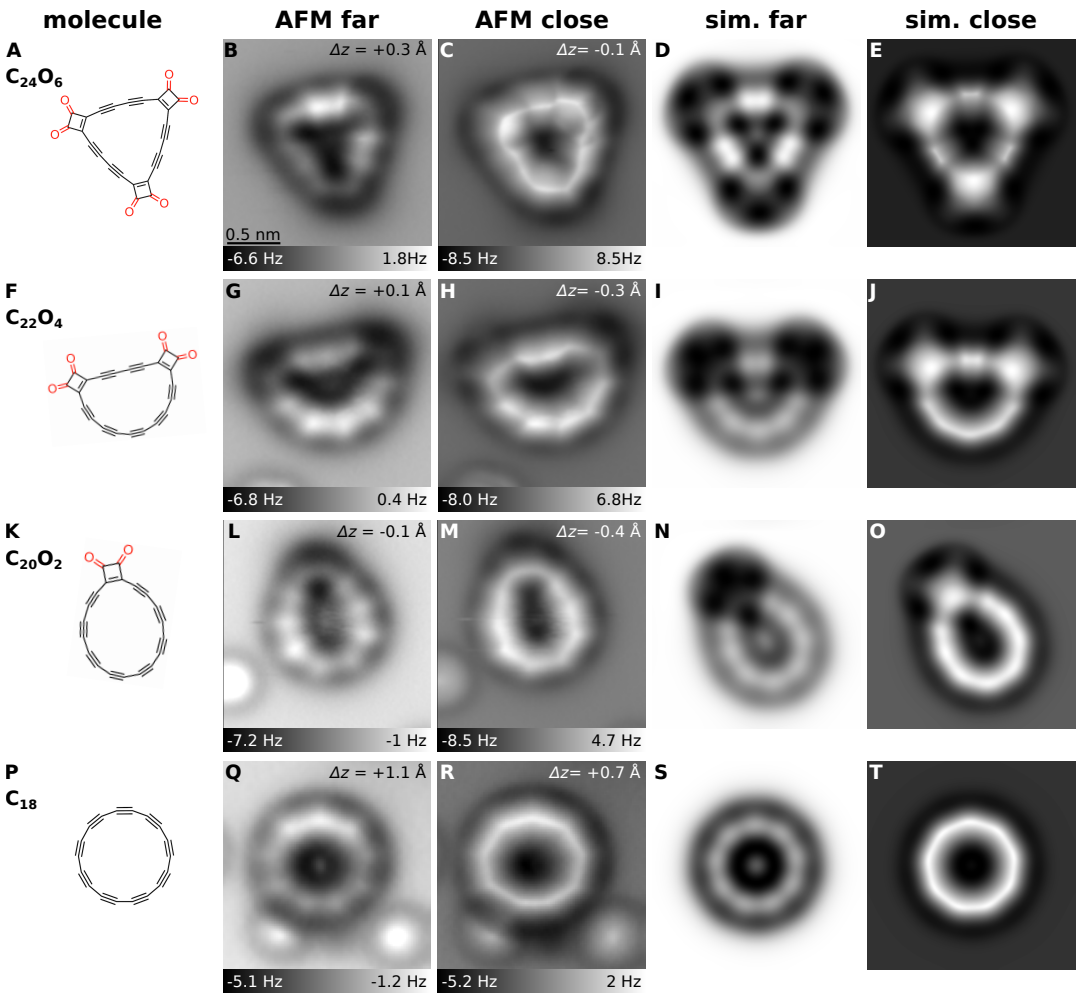

Figure 3: Precursor and products generated by tip-induced decarbonylation. Structures (1st column) and AFM images (2nd and 3rd column) recorded with a CO-functionalized tip at different tip offsets Δz, with respect to an STM set point of $I = 0.5$ pA, $V = 0.2$ V above the NaCl surface, showing (**A**–**E**) precursor, (**F**–**J** and **K**–**O**) most frequently observed intermediates and (**P**–**T**) cyclo[18]carbon. The bright features at the lower part in L, M, Q and R correspond to individual CO molecules. Simulated AFM images (4th and 5th column) based on gas-phase DFT calculated geometries. The difference in probe height in "sim. far" to "sim. close" corresponds to the respective differences in "AFM far" and "AFM close". The same scale bar as in (B) applies to all experimental and simulated AFM images.

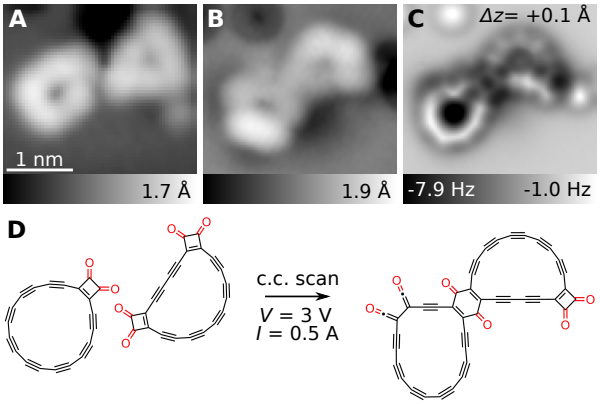

Figure 4: Molecular fusion by atom manipulation. (**A**) STM image of two neighboring intermediates, identified as $C_{22}O_4$ and $C_{20}O_2$. Imaging the area at constant current (c.c.) with a set point of $V = 3$ V, $I = 0.5$ pA resulted in the reaction between the molecules. (**B**, **C**) STM and AFM image of the resulting fused molecule, respectively. (**D**) Proposed reaction scheme. See supplementary material for further examples of molecular fusion reactions.